SLAC-PUB-14772

CERN-PH-EP-2009-005
2 March 2009

Precise measurement of the $K^{\pm} \to \pi^{\pm} e^{+} e^{-}$ decay

The NA48/2 Collaboration

J.R. Batley, A.J. Culling, G. Kalmus, C. Lazzeroni [1], D.J. Munday, M.W. Slater [1], S.A. Wotton
Cavendish Laboratory, University of Cambridge, Cambridge, CB3 0HE, UK [2]

R. Arcidiacono [3], G. Bocquet, N. Cabibbo [4], A. Ceccucci, D. Cundy [5], V. Falaleev, M. Fidecaro, L. Gatignon, A. Gonidec, W. Kubischta, A. Norton [6], A. Maier, M. Patel, A. Peters
CERN, CH-1211 Genève 23, Switzerland

S. Balev [7], P.L. Frabetti, E. Goudzovski [*1], P. Hristov [8], V. Kekelidze, V. Kozhuharov [9], L. Litov, D. Madigozhin, E. Marinova [*10], N. Molokanova, I. Polenkevich, Yu. Potrebenikov, S. Stoynev [11], A. Zinchenko
Joint Institute for Nuclear Research, 141980 Dubna, Moscow region, Russia

E. Monnier [12], E. Swallow, R. Winston
The Enrico Fermi Institute, The University of Chicago, Chicago, IL 60126, USA

P. Rubin [13], A. Walker
Department of Physics and Astronomy, University of Edinburgh, JCMB King's Buildings, Mayfield Road, Edinburgh, EH9 3JZ, UK

W. Baldini, A. Cotta Ramusino, P. Dalpiaz, C. Damiani, M. Fiorini [8], A. Gianoli, M. Martini, F. Petrucci, M. Savrié, M. Scarpa, H. Wahl
Dipartimento di Fisica dell'Università e Sezione dell'INFN di Ferrara, I-44100 Ferrara, Italy

A. Bizzeti [14], M. Calvetti, E. Celeghini, E. Iacopini, M. Lenti, F. Martelli [15], G. Ruggiero [7], M. Veltri [15]
Dipartimento di Fisica dell'Università e Sezione dell'INFN di Firenze, I-50125 Firenze, Italy

M. Behler, K. Eppard, K. Kleinknecht, P. Marouelli, L. Masetti [16], U. Moosbrugger, C. Morales Morales, B. Renk, M. Wache, R. Wanke, A. Winhart
Institut für Physik, Universität Mainz, D-55099 Mainz, Germany [17]

D. Coward [18], A. Dabrowski, T. Fonseca Martin [19], M. Shieh, M. Szleper, M. Velasco, M.D. Wood [20]
Department of Physics and Astronomy, Northwestern University, Evanston, IL 60208, USA

G. Anzivino, P. Cenci, E. Imbergamo, A. Nappi, M. Pepe, M.C. Petrucci, M. Piccini, M. Raggi [21], M. Valdata-Nappi
Dipartimento di Fisica dell'Università e Sezione dell'INFN di Perugia, I-06100 Perugia, Italy

C. Cerri, R. Fantechi
Sezione dell'INFN di Pisa, I-56100 Pisa, Italy

G. Collazuol, L. DiLella, G. Lamanna, I. Mannelli, A. Michetti
Scuola Normale Superiore e Sezione dell'INFN di Pisa, I-56100 Pisa, Italy

Work supported in part by US Department of Energy contract DE-AC02-76SF00515.

SLAC National Accelerator Laboratory, Menlo Park, CA 94025

F. Costantini, N. Doble, L. Fiorini [22], S. Giudici, G. Pierazzini, M. Sozzi, S. Venditti
Dipartimento di Fisica dell'Università e Sezione dell'INFN di Pisa, I-56100 Pisa Italy

B. Bloch-Devaux, C. Cheshkov [8], J.B. Chèze, M. De Beer, J. Derré, G. Marel, E. Mazzucato, B. Peyaud, B. Vallage
DSM/IRFU – CEA Saclay, F-91191 Gif-sur-Yvette, France

M. Holder, M. Ziolkowski
Fachbereich Physik, Universität Siegen, D-57068 Siegen, Germany [23]

S. Bifani [24], C. Biino, N. Cartiglia, M. Clemencic [8], S. Goy Lopez [25], F. Marchetto
Dipartimento di Fisica Sperimentale dell'Università e Sezione dell'INFN di Torino, I-10125 Torino, Italy

H. Dibon, M. Jeitler, M. Markytan, I. Mikulec, G. Neuhofer, L. Widhalm
Österreichische Akademie der Wissenschaften, Institut für Hochenergiephysik, A-10560 Wien, Austria [26]

Accepted for publication in Physics Letters B.

*Corresponding authors, emails: eg@hep.ph.bham.ac.uk, evelina.marinova@cern.ch
[1]University of Birmingham, Edgbaston, Birmingham, B15 2TT, UK
[2]Funded by the UK Particle Physics and Astronomy Research Council
[3]Dipartimento di Fisica Sperimentale dell'Università e Sezione dell'INFN di Torino, I-10125 Torino, Italy
[4]Università di Roma "La Sapienza" e Sezione dell'INFN di Roma, I-00185 Roma, Italy
[5]Istituto di Cosmogeofisica del CNR di Torino, I-10133 Torino, Italy
[6]Dipartimento di Fisica dell'Università e Sezione dell'INFN di Ferrara, I-44100 Ferrara, Italy
[7]Scuola Normale Superiore, I-56100 Pisa, Italy
[8]CERN, CH-1211 Genève 23, Switzerland
[9]Faculty of Physics, University of Sofia "St. Kl. Ohridski", 5 J. Bourchier Blvd., 1164 Sofia, Bulgaria
[10]Sezione dell'INFN di Perugia, I-06100 Perugia, Italy
[11]Northwestern University, 2145 Sheridan Road, Evanston, IL 60208, USA
[12]Centre de Physique des Particules de Marseille, IN2P3-CNRS, Université de la Méditerranée, Marseille, France
[13]Department of Physics and Astronomy, George Mason University, Fairfax, VA 22030, USA
[14]Istituto di Fisica, Università di Modena e Reggio Emilia, I-41100 Modena, Italy
[15]Istituto di Fisica, Università di Urbino, I-61029 Urbino, Italy
[16]Physikalisches Institut, Universität Bonn, D-53115 Bonn, Germany
[17]Funded by the German Federal Minister for Education and research under contract 05HK1UM1/1
[18]SLAC, Stanford University, Menlo Park, CA 94025, USA
[19]Royal Holloway, University of London, Egham Hill, Egham, TW20 0EX, UK
[20]UCLA, Los Angeles, CA 90024, USA
[21]Laboratori Nazionali di Frascati, via E. Fermi, 40, I-00044 Frascati (Rome), Italy
[22]Institut de Física d'Altes Energies, UAB, E-08193 Bellaterra (Barcelona), Spain
[23]Funded by the German Federal Minister for Research and Technology (BMBF) under contract 056SI74
[24]University of Bern, Institute for Theoretical Physics, Sidlerstrasse 5, CH-3012 Bern, Switzerland
[25]Centro de Investigaciones Energeticas Medioambientales y Tecnologicas, E-28040 Madrid, Spain
[26]Funded by the Austrian Ministry for Traffic and Research under the contract GZ 616.360/2-IV GZ 616.363/2-VIII, and by the Fonds für Wissenschaft und Forschung FWF Nr. P08929-PHY

Abstract

A sample of 7253 $K^{\pm} \to \pi^{\pm}e^{+}e^{-}(\gamma)$ decay candidates with 1.0% background contamination has been collected by the NA48/2 experiment at the CERN SPS, which allowed a precise measurement of the decay properties. The branching ratio in the full kinematic range was measured to be BR = $(3.11 \pm 0.12) \times 10^{-7}$, where the uncertainty includes also the model dependence. The shape of the form factor $W(z)$, where $z = (M_{ee}/M_K)^2$, was parameterized according to several models, and, in particular, the slope δ of the linear form factor $W(z) = W_0(1+\delta z)$ was determined to be $\delta = 2.32 \pm 0.18$. A possible CP violating asymmetry of K^+ and K^- decay widths was investigated, and a conservative upper limit of 2.1×10^{-2} at 90% CL was established.

Introduction

Radiative nonleptonic kaon decays represent a source of information on the structure of the weak interactions at low energies. The flavour-changing neutral current process $K^{\pm} \to \pi^{\pm}e^+e^-$, induced at one-loop level in the Standard Model and highly suppressed by the GIM mechanism [1], is of particular interest. The $K^{\pm} \to \pi^{\pm}l^+l^-$ processes have been described by the Chiral Perturbation Theory (ChPT) [2]; several models predicting the form factor characterizing the dilepton invariant mass spectrum, and thus the decay rate, have been proposed [3, 4, 5].

The first observation of the $K^+ \to \pi^+e^+e^-$ process was made at the CERN PS more than 30 years ago [6], followed more recently by BNL E777 [7] and E865 [8] measurements. The most precise of these, E865, based on a sample of 10300 candidates with 1.2% background, allowed a detailed analysis of the decay form factor and rate, and a test of the next-to-leading order ChPT calculation [3].

In this paper, a new precise measurement of the $K^{\pm} \to \pi^{\pm}e^+e^-$ decay is reported, based on the full data set collected in 2003–2004 by the NA48/2 experiment at the CERN SPS. In addition to spectrum and rate studies, the first observation of the K^- decay allowed setting an upper limit on the charge asymmetry of $K^+ \to \pi^+e^+e^-$ and $K^- \to \pi^-e^+e^-$ decay rates, which can be related to CP violation.

1 The NA48/2 experiment

The NA48/2 experiment, specifically designed for charge asymmetry measurements [9], uses simultaneous K^+ and K^- beams produced by 400 GeV/c primary SPS protons impinging on a beryllium target. Charged particles with momentum (60 ± 3) GeV/c are selected by an achromatic system of four dipole magnets with zero total deflection ('achromat'), which splits the two beams in the vertical plane and then recombines them on a common axis. The beams pass through momentum defining collimators and a series of four quadrupoles designed to focus the beams at the detector. Finally the two beams are again split in the vertical plane and recombined in a second achromat. The layout of the beams and detectors is shown schematically in Fig. 1.

The beams then enter the fiducial decay volume housed in a 114 m long cylindrical vacuum tank with a diameter of 1.92 m, extended to 2.4 m after the first 65 m. Both beams follow the same path in the decay volume: their axes coincide within 1 mm, while the transverse size of the beams is about 1 cm. With 7×10^{11} protons incident on the target per SPS spill of 4.8 s duration, the positive (negative) beam flux at the entrance of the decay volume is 3.8×10^7 (2.6×10^7) particles per pulse, of which 5.7% (4.9%) are K^+ (K^-). The K^+/K^- flux ratio is 1.79. The fraction of beam kaons decaying in the decay volume at nominal momentum is 22%.

A detailed description of the NA48 detector can be found in [10]. The decay volume is followed by a magnetic spectrometer housed in a tank filled with helium at nearly atmospheric pressure, separated from the vacuum tank by a thin ($0.31\%X_0$) Kevlar composite window. A thin-walled aluminium beam pipe of 16 cm outer diameter traversing the centre of the spectrometer (and all the following detectors) allows the undecayed beam particles and the muon halo from decays of beam pions to continue their path in vacuum. The spectrometer consists of four drift chambers (DCH): DCH1, DCH2 located upstream, and

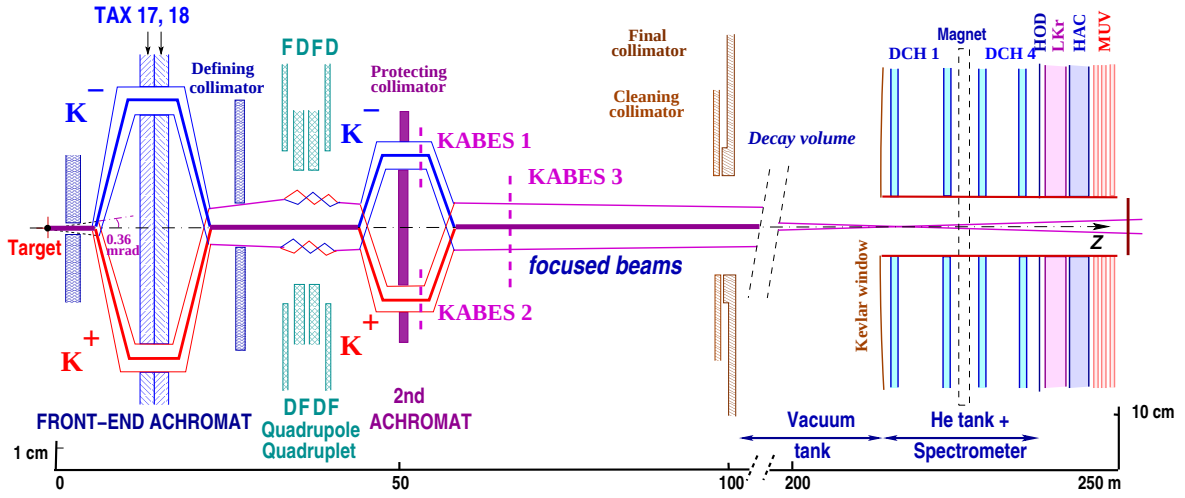

Figure 1: Schematic lateral view of the NA48/2 beam line (TAX17,18: motorized beam dump/collimators used to select the momentum of the K^+ and K^- beams; FDFD/DFDF: focusing set of quadrupoles, KABES1–3: beam spectrometer stations not used in this analysis), decay volume, and detector (DCH1–4: drift chambers, HOD: hodoscope, LKr: EM calorimeter, HAC: hadron calorimeter, MUV: muon veto). Note that the vertical scales are different in the two parts of the figure.

DCH3, DCH4 downstream of a dipole magnet. The magnet provides a horizontal transverse momentum kick $\Delta p = 120$ MeV/c for charged particles. Each DCH is composed of eight planes of sense wires. The spatial resolution of each DCH is $\sigma_x = \sigma_y = 90$ μm. The nominal spectrometer momentum resolution is $\sigma_p/p = (1.02 \oplus 0.044 \cdot p)\%$ (p in GeV/c).

The magnetic spectrometer is followed by a plastic scintillator hodoscope (HOD) used to produce fast trigger signals and to provide precise time measurements of charged particles. The hodoscope has a regular octagonal shape with a transverse size of about 2.4 m, and consists of a plane of horizontal and a plane of vertical strip-shaped counters.

The HOD is followed by a liquid krypton electromagnetic calorimeter (LKr) used for photon detection and particle identification. It is an almost homogeneous ionization chamber with an active volume of 7 m^3 of liquid krypton, segmented transversally into 13248 projective cells, 2×2 cm^2 each, and with no longitudinal segmentation. The calorimeter is $27X_0$ deep and has an energy resolution $\sigma(E)/E = 0.032/\sqrt{E} \oplus 0.09/E \oplus 0.0042$ (E in GeV). Spatial resolution for an isolated electromagnetic shower is $\sigma_x = \sigma_y = 0.42/\sqrt{E} \oplus 0.06$ cm (E in GeV) for the transverse coordinates x and y.

The LKr is followed by a hadronic calorimeter (HAC) and a muon detector (MUV), both not used in the present analysis.

2 Data analysis

The $K^\pm \to \pi^\pm e^+ e^-$ rate is measured relative to the more abundant $K^\pm \to \pi^\pm \pi^0_D$ normalisation channel (where $\pi^0_D \to e^+ e^- \gamma$ is the so called Dalitz decay). The final states of the signal and normalisation channels contain identical sets of charged particles. Thus electron and pion identification efficiencies, potentially representing a significant source of systematic uncertainties, cancel in the first order.

Monte Carlo simulation

In order to compute acceptances for signal, normalisation and background channels, a detailed GEANT3-based [11] Monte Carlo (MC) simulation is employed, which includes full detector geometry and material description, stray magnetic fields, DCH local inefficiencies and misalignment, detailed simulation of the kaon beam line, and time variations of the above throughout the running period.

Event selection

Three-track vertices (compatible with the topology of $K^\pm \to \pi^\pm e^+ e^-$ and $K^\pm \to \pi^\pm \pi^0_D$ decays) are reconstructed by extrapolation of track segments from the upstream part of the spectrometer back into the decay volume, taking into account the measured Earth's magnetic field, stray fields due to magnetization of the vacuum tank, and multiple scattering.

A large part of the selection is common to the signal and normalisation modes. It requires the presence of a vertex satisfying the following criteria.

- Vertex longitudinal position is inside fiducial decay volume: $Z_{\rm vertex} > Z_{\rm final\ collimator}$.
- The vertex tracks are required to be consistent in time (within a 10 ns time window) and consistent with the trigger time, to be in DCH, HOD and LKr geometric acceptance, and to have momenta in the range 5 GeV/$c < p <$ 50 GeV/c. Track separations are required to exceed 2 cm in the DCH1 plane to suppress photon conversions, and to exceed 15 cm in the LKr front plane to minimize particle misidentification due to shower overlaps.
- Total charge of the three tracks: $Q = \pm 1$.
- Particle identification is performed using the ratio E/p of energy deposition of the particle in the LKr calorimeter to its momentum measured by the spectrometer. The vertex is required to be composed of one π candidate ($E/p < 0.85$), and a pair of oppositely charged $e^\pm$ candidates ($E/p > 0.95$). No discrimination of pions against muons is performed.

If several vertices satisfy the above conditions, the one with the best vertex fit quality is considered. The $K^\pm \to \pi^\pm e^+ e^-$ candidates are selected by applying the following criteria to the reconstructed kinematic variables.

- $\pi^\pm e^+ e^-$ momentum within the beam nominal range: 54 GeV/$c < |\vec{p}_{\pi ee}| <$ 66 GeV/c.
- $\pi^\pm e^+ e^-$ transverse momentum with respect to the beam trajectory (which is precisely measured using the the concurrently acquired $K^\pm \to 3\pi^\pm$ sample): $p_T^2 < 0.5 \times 10^{-3}$ (GeV/c)^2.
- Kinematic suppression of the main background channel $K^\pm \to \pi^\pm \pi^0_D$ (and other minor backgrounds induced by π^0_D and $\pi^0_{DD} \to 4e^\pm$ decays) by requiring the e^+e^- mass to be above the π^0 mass: $z = (M_{ee}/M_K)^2 > 0.08$, which approximately corresponds to $M_{ee} > 140$ MeV/c^2, and leads to an unavoidable loss of $\sim 30\%$ of the signal sample.

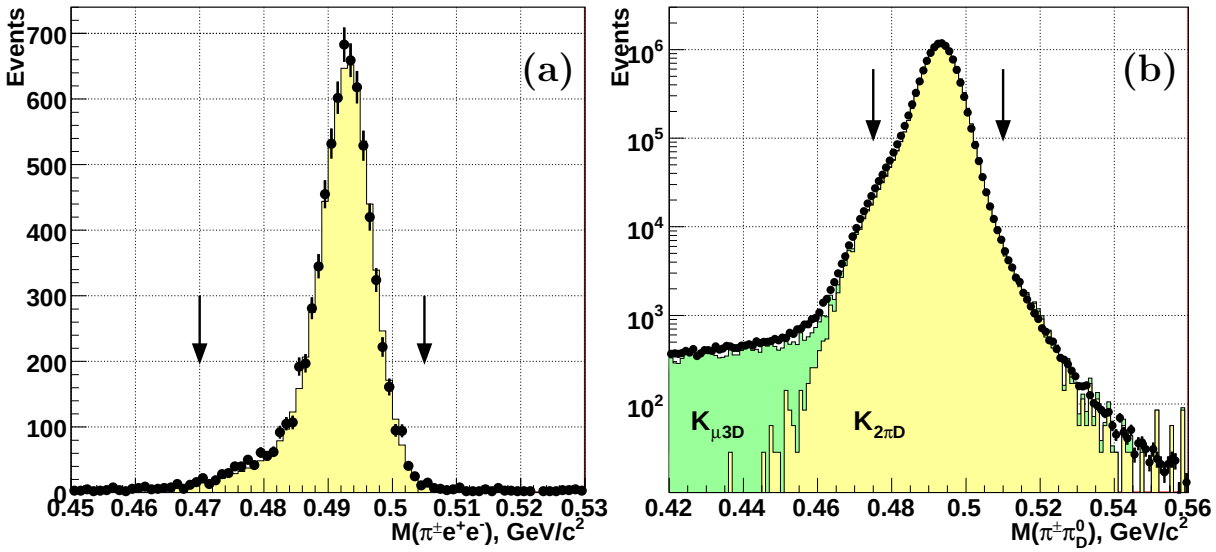

Figure 2: (a) Reconstructed spectrum of $\pi^\pm e^+ e^-$ invariant mass: data (dots) and MC simulation (filled area). Note the description of the radiative mass tail by the PHOTOS simulation. (b) Reconstructed spectrum of $\pi^\pm \pi^0_D$ invariant mass: data (dots) and MC simulations of $K^\pm \to \pi^\pm \pi^0_D$ signal and $K^\pm \to \pi^0_D \mu^\pm \nu$ background (filled areas). Signal regions are indicated with arrows.

- $\pi^\pm e^+ e^-$ invariant mass: 470 MeV/c^2 $< M_{\pi ee} <$ 505 MeV/c^2. The signal region, asymmetric with respect to the nominal kaon mass (Fig. 2a), includes a part of the radiative mass tail. The lower mass limit of 470 MeV/c^2 corresponds to an upper cutoff $E_\gamma < 23.1$ MeV for the energy of a single directly undetectable soft radiative photon, and is chosen as a trade-off between making an inclusive analysis, and keeping the background reasonably small.

No restrictions are applied to the $K^\pm \to \pi^\pm e^+ e^-$ sample on the additional energy deposition in the LKr calorimeter, the reason being two-fold: 1) to avoid bias due to the radiative $K^\pm \to \pi^\pm e^+ e^- \gamma$ decays (with predominantly soft photons, which makes the LKr response difficult to simulate); 2) to decrease sensitivity to accidental activity.

For the $K^\pm \to \pi^\pm \pi^0_D$ normalisation mode candidates, the presence of a LKr energy deposition cluster (photon candidate) satisfying the following principal criteria is required.

- Reconstructed cluster energy $E > 3$ GeV, cluster time consistent with the vertex time, sufficient transverse separations from track impact points at the LKr plane ($R_{\pi\gamma} > 30$ cm, $R_{e\gamma} > 10$ cm).
- $e^+ e^- \gamma$ invariant mass compatible with a π^0_D decay: $|M_{ee\gamma} - M_{\pi^0}| < 10$ MeV/c^2.
- The same conditions on reconstructed $\pi^\pm e^+ e^- \gamma$ total and transverse momenta as used for $\pi^\pm e^+ e^-$ momentum in the $K^\pm \to \pi^\pm e^+ e^-$ selection.
- $\pi^\pm e^+ e^- \gamma$ invariant mass: 475 MeV/c^2 $< M_{\pi ee\gamma} <$ 510 MeV/c^2.

Signal sample

The reconstructed $\pi^{\pm}e^{+}e^{-}$ invariant mass spectrum is presented in Fig. 2a. The measured $M_{\pi ee}$ resolution is $\sigma_{\pi ee} = 4.2$ MeV/c^2, in agreement with MC simulation. The $e^{+}e^{-}$ invariant mass resolution computed by MC simulation is $\sigma_{ee} = 2.3$ MeV/c^2. The number of $K^{\pm} \to \pi^{\pm}e^{+}e^{-}(\gamma)$ decay candidates in the signal region is $N_{\pi ee} = 7253$, out of which 4613 (2640) are K^{+} (K^{-}) candidates. The residual background sources after the kinematical suppression of the π^0_D and π^0_{DD} decays are the following.

- Kaon decays with a π^0 in the final state followed by a $\pi^0_D \to e^{+}e^{-}\gamma$ decay and particle misidentification ($e^{\pm}$ identified as $\pi^{\pm}$ or vice versa). Two dominant contributions identified with MC simulations are (1) $K^{\pm} \to \pi^{\pm}\pi^0_D$ with misidentified $e^{\pm}$ and $\pi^{\pm}$; (2) $K^{\pm} \to \pi^0_D e^{\pm}\nu$ with a misidentified $e^{\pm}$ from the π^0_D decay. The two contributions are of similar size, which means that about 75% of electron candidates in this sample are genuine electrons, and the rest are misidentified pions.

- Kaon decays with two $e^{+}e^{-}$ pairs in the final state resulting from either $\pi^0_{D(D)}$ decays or external γ conversions, only a single lepton from each $e^{+}e^{-}$ pair constituting the best vertex, without particle misidentification involved. All electron candidates in this sample are genuine electrons.

Backgrounds can be reliably estimated and subtracted using the data sample itself. For the first of the above background types, the expected kinematic distribution of the lepton number violating "same lepton sign" $\pi^{\mp}e^{\pm}e^{\pm}$ candidates is identical to that of background events (up to a negligible acceptance correction). For the second background type, the expected sum of distributions of the same lepton sign candidates and the $\pi^{\pm}e^{\pm}e^{\pm}$ candidates with the unphysical total charge $|Q| = 3$ is similarly identical to that of background events. Background contamination is estimated using the sum of the numbers of same lepton sign candidates $N_{ss} = 55$, and $|Q| = 3$ candidates $N_{q3} = 16$ as $(N_{ss} + N_{q3})/N_{\pi ee} = (1.0 \pm 0.1_{\mathrm{stat.}})\%$.

A cross check of the composition of same lepton sign and $|Q| = 3$ samples using a tighter electron identification (based not only on E/p but also on shower properties and track-cluster matching) confirms the expected fractions of genuine electrons among the electron candidates.

Normalisation sample

The reconstructed $\pi^{\pm}e^{+}e^{-}\gamma$ invariant mass spectrum is presented in Fig. 2b. The number of $K^{\pm} \to \pi^{\pm}\pi^0_D$ candidates in the signal region is $N_{2\pi} = 1.212 \times 10^7$, which corresponds to the number of kaon decays in the fiducial decay volume of about $N_K = 1.7 \times 10^{11}$. The only significant background source is the semileptonic $K^{\pm} \to \pi^0_D \mu^{\pm}\nu$ decay. Its contribution is not suppressed by particle identification requirements, since no π/μ separation is performed. The background contamination in the signal region is estimated to be 0.15% by MC simulation.

Trigger chain and its efficiency

Both $K^{\pm} \to \pi^{\pm}e^{+}e^{-}$ and $K^{\pm} \to \pi^{\pm}\pi^0_D$ samples are recorded via a two-level trigger chain designed to collect the $K^{\pm} \to 3\pi^{\pm}$ decays. At the first level (L1), the HOD surface is logically subdivided into 16 non-overlapping square regions; a coincidence of hits in the two planes of the HOD is required to occur in at least two such regions. The second level

(L2) is based on a hardware system computing coordinates of hits from DCH drift times, and a farm of asynchronous processors performing fast track reconstruction and running a selection algorithm, which basically requires the presence of at least two tracks consistent with a common origin in the decay volume (closest distance of approach less than 5 cm). L1 triggers not satisfying this condition are examined further and accepted nevertheless if there is a reconstructed track not kinematically compatible with a $\pi^\pm\pi^0$ decay of a $K^\pm$ having momentum of 60 GeV/c directed along the beam axis.

The NA48/2 analysis strategy for non-rare decay modes involves direct measurement of the trigger efficiencies using control data samples of downscaled low bias triggers collected simultaneously with the main triggers. However direct measurements are not possible for the $K^\pm \to \pi^\pm e^+ e^-$ events due to very limited sizes of the corresponding control samples. Dedicated simulations of L1 and L2 performance were used instead. The sources of the trigger inefficiency are the local inefficiencies of the HOD and the DCHs, which were mapped using special muon runs and the $K^\pm \to \pi^\pm\pi^+\pi^-$ data, and included into the simulations. The simulated efficiencies and their kinematic dependencies were compared against measurements for the abundant $K^\pm \to \pi^\pm\pi^0_D$ and $K^\pm \to \pi^\pm\pi^+\pi^-$ decays in order to validate the simulations; simulated values of trigger efficiencies agree with the measurements to a level of a few 10^{-4} units.

The simulated values of L1 and L2 inefficiencies for the selected $K^\pm \to \pi^\pm\pi^0_D$ sample are $\varepsilon_{L1} = 0.37\%$, $\varepsilon_{L2} = 0.80\%$. The values of the integral trigger inefficiencies for the $K^\pm \to \pi^\pm e^+ e^-$ sample depend on the a priori unknown form factor; the corrections are applied differentially in bins of dilepton invariant mass M_{ee}. Indicative values of inefficiencies for a realistic linear form factor with a slope $\delta = 2.3$ are $\varepsilon_{L1} = 0.06\%$, $\varepsilon_{L2} = 0.42\%$. The $K^\pm \to \pi^\pm\pi^0_D$ sample is affected by a larger trigger inefficiency due to the smaller invariant masses M_{ee}, which means that the lepton trajectories are geometrically closer. Similarly, the inefficiency is enhanced for $K^\pm \to \pi^\pm e^+ e^-$ events at low M_{ee}.

Theoretical input

The decay is supposed to proceed through single virtual photon exchange, resulting in a spectrum of the $z = (M_{ee}/M_K)^2$ kinematic variable sensitive to the form factor $W(z)$ [2]:

$$\frac{d\Gamma}{dz} = \frac{\alpha^2 M_K}{12\pi(4\pi)^4}\lambda^{3/2}(1, z, r_\pi^2)\sqrt{1-4\frac{r_e^2}{z}}\left(1+2\frac{r_e^2}{z}\right)|W(z)|^2, \qquad (1)$$

where $r_e = m_e/M_K$, $r_\pi = m_\pi/M_K$, and $\lambda(a,b,c) = a^2+b^2+c^2-2ab-2ac-2bc$. On the other hand, the spectrum of the angle $\theta_{\pi e}$ between π and e^+ in the e^+e^- rest frame is $d\Gamma/d\theta_{\pi e} = C\sin^2\theta_{\pi e}$, C = const, and is not sensitive to $W(z)$. The expression for two-dimensional decay density can be found for instance in [5].

The following parameterizations of the form factor $W(z)$ are considered in the present analysis.

1. Linear: $W(z) = G_F M_K^2 f_0(1+\delta z)$ with free normalisation and slope (f_0, δ). Decay rate and z spectrum are sensitive to $|f_0|$, not to its sign.

2. Next-to-leading order ChPT [3]: $W(z) = G_F M_K^2(a_+ + b_+ z) + W^{\pi\pi}(z)$ with free parameters (a_+, b_+) and an explicitly calculated pion loop term $W^{\pi\pi}(z)$ given in [3].

3. Combined framework of ChPT and large-N_c QCD [4]: the form factor is parameterized as $W(z) \equiv W(\tilde{\mathrm{w}}, \beta, z)$ with free parameters $(\tilde{\mathrm{w}}, \beta)$, see also the Appendix.

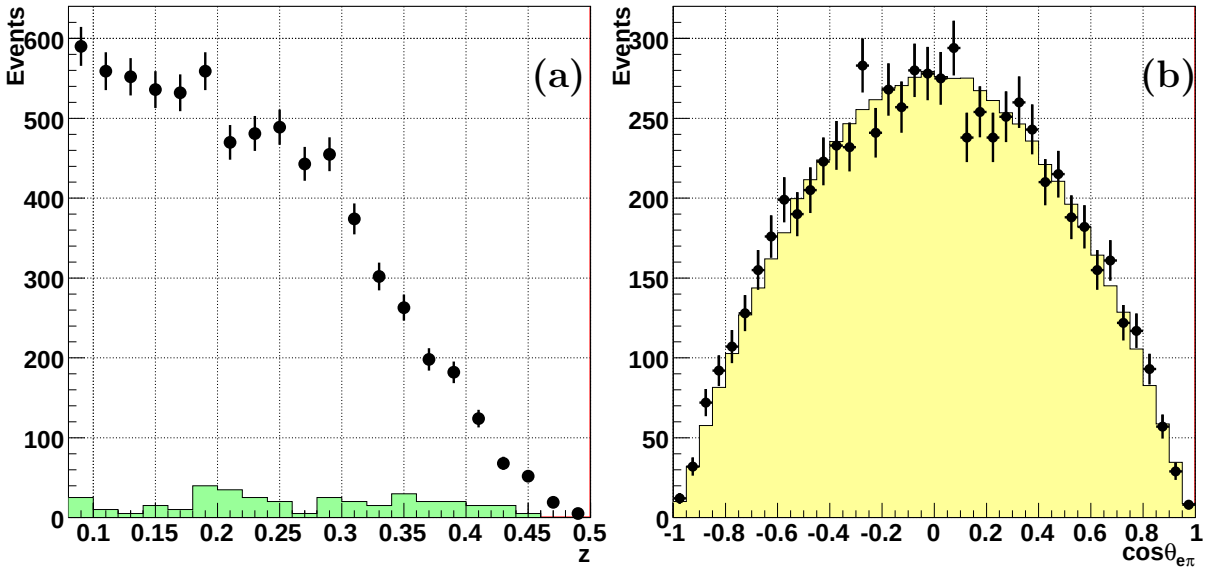

Figure 3: (a) z spectrum of the selected $K^{\pm} \to \pi^{\pm}e^{+}e^{-}$ candidates. Filled area: background estimated with same lepton sign and $|Q| = 3$ events, multiplied by a factor of 5 for visibility. (b) $\theta_{\pi e}$ spectrum of the selected candidates (dots) and its comparison to MC assuming vector interaction (filled area).

4. ChPT parameterization [5] involving meson form factors: $W(z) \equiv W(M_a, M_\rho, z)$. The resonance masses ($M_a$, M_ρ) are treated as free parameters in the present analysis.

The goal of the analysis is measuring the form factor parameters in the framework of each of the above models, and the computation of the corresponding branching ratios $\mathrm{BR}_{1,2,3,4}$ by integration of (1) normalised to full $K^{\pm}$ decay width Γ_K [14].

The Coulomb correction factor is taken into account following [13] (eq. 20). The effects of radiative corrections to the $K^{\pm} \to \pi^{\pm}e^{+}e^{-}$ process are evaluated using the PHOTOS [12] simulation of the $K^{\pm} \to \pi^{\pm}\gamma^{*} \to \pi^{\pm}e^{+}e^{-}$ decay chain. The results are cross-checked using a generalized computation for a multi-body meson decay [13] (eq. 19). In addition to affecting the values of the model parameters, radiative corrections are crucial for the extrapolation of the branching ratio from the limited $M_{\pi ee}$ (equivalently, E_γ) signal region to the full kinematic region; according to the above models for radiative corrections, about 6% of the total $K^{\pm} \to \pi^{\pm}e^{+}e^{-}(\gamma)$ decay rate fall outside the signal region $E_\gamma < 23.1$ MeV.

Fitting procedure

The observed spectra of the data events in z (in the visible region $z > 0.08$) and $\cos\theta_{\pi e}$ variables are presented in Fig. 3. The latter spectrum, which contains no information about $W(z)$, is compared to the MC expectation, demonstrating a good agreement.

The values of $d\Gamma_{\pi ee}/dz$ in the centre of each i-bin of z, which can be directly compared to the theoretical predictions (1), are then computed as

$$(d\Gamma_{\pi ee}/dz)_i = \frac{N_i - N_i^B}{N_{2\pi}} \cdot \frac{A_{2\pi}(1-\varepsilon_{2\pi})}{A_i(1-\varepsilon_i)} \cdot \frac{1}{\Delta z} \cdot \frac{\hbar}{\tau_K} \cdot \mathrm{BR}(K^{\pm} \to \pi^{\pm}\pi^0) \cdot \mathrm{BR}(\pi^0_D). \qquad (2)$$

Here N_i and N_i^B are the numbers of observed $K^{\pm} \to \pi^{\pm}e^{+}e^{-}$ candidates and background events in the i-th bin, $N_{2\pi}$ is the number of $K^{\pm} \to \pi^{\pm}\pi^0_D$ events (with background

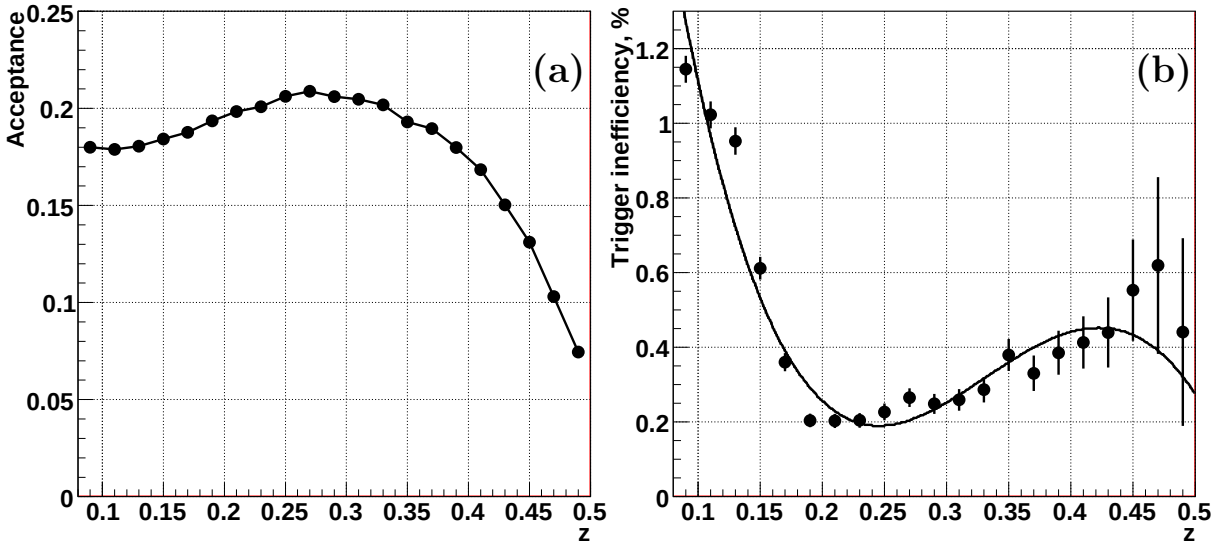

Figure 4: (a) Geometrical acceptances A_i and (b) trigger inefficiencies ε_i for the $K^\pm \to \pi^\pm e^+ e^-$ sample in bins of z, both obtained by MC simulations. The kinematical dependence of the trigger inefficiency is mainly due to enhancement of L1 inefficiency for event topologies with two tracks hitting the same HOD segment. The polynomial superimposed on Figure (b) is drawn only to guide the eye.

subtracted), A_i and ε_i are geometrical acceptance and trigger inefficiency in the i-th bin for the signal sample (computed by MC simulation, both presented in Fig. 4), $A_{2\pi} = 2.95\%$ and $\varepsilon_{2\pi} = 1.17\%$ are those for $K^\pm \to \pi^\pm \pi^0_D$ events, Δz is the z bin width, and is set to 0.02. The external inputs are the kaon lifetime $\tau_K = (1.2380 \pm 0.0021) \times 10^{-8}$ s, and branching ratios of the normalisation decay modes $\mathrm{BR}(K^\pm \to \pi^\pm \pi^0) = (20.68 \pm 0.13)\%$, $\mathrm{BR}(\pi^0_D) = (1.198 \pm 0.032)\%$ [14].

While the simulated values of geometric acceptances and trigger efficiencies are subject to relatively large systematic uncertainties (discussed in the following section), their ratios $A_i/A_{2\pi}$ and $(1-\varepsilon_i)/(1-\varepsilon_{2\pi})$ appearing in (2) are affected by these uncertainties to a lesser extent due to cancellations of most systematic effects.

The computed values of $d\Gamma_{\pi ee}/dz$ vs z and the results of the fits to the four considered models are presented in Fig. 5a. The corresponding squared form factors $|W(z)|^2$ normalized by a condition $|W(0)| = 1$ are presented in Fig. 5b.

Branching ratios $\mathrm{BR}(K^\pm \to \pi^\pm e^+ e^-)$ in the full kinematic range corresponding to each model are computed using the measured value of the model parameters, their statistical uncertainties, and correlation matrices. In addition, a model-independent branching ratio $\mathrm{BR_{mi}}$ in the visible kinematic region $z > 0.08$ is computed by integration of $d\Gamma_{\pi ee}/dz$. $\mathrm{BR_{mi}}$ differs from each of the model-dependent BRs computed in the visible z range by less than 0.01×10^{-7}. The differences between the model-dependent BRs come from the region $z < 0.08$, as can be seen in Fig. 5a.

Systematic uncertainties

Particle identification. Imperfect MC description of electron and pion identification inefficiencies f_e and f_π can bias the result only due to the momentum dependence of f_e and f_π, due to identical charged particle composition, but differing π and e momentum

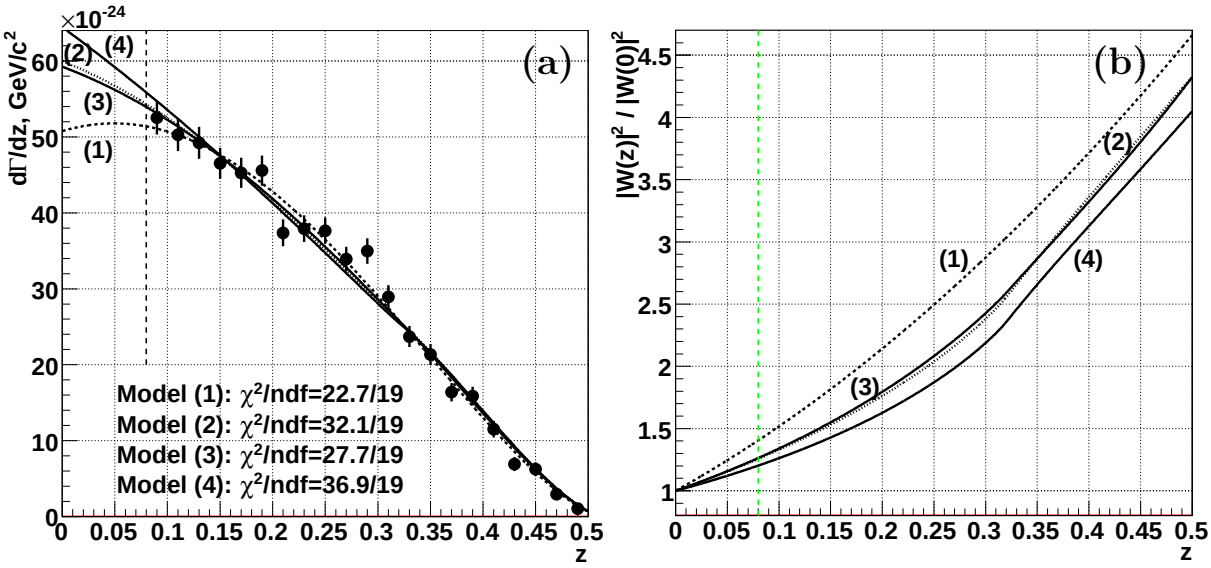

Figure 5: (a) $d\Gamma_{\pi ee}/dz$ (background subtracted, corrected for trigger efficiency) and fit results according to the four considered models. (b) Squared form factors $|W(z)|^2$ for each model normalized by a condition $|W(0)| = 1$.

spectra of the signal and normalisation modes. Inefficiencies were measured with the data to be in the ranges $1.6\% < f_\pi < 1.7\%$ and $1.1\% < f_e < 1.7\%$, depending in momentum. Systematic uncertainties due to these momentum dependencies not perfectly described by MC were conservatively estimated assuming momentum-independent MC f_e and f_π.

Beam line description. Despite the careful simulation of the beamline including time variations of its parameters, the residual discrepancies of data and MC beam geometries and spectra may bias the results. To evaluate the related systematic uncertainties, variations of the results with respect to variations of cuts on track momenta, LKr cluster energies, total and transverse momenta of the $\pi^\pm e^+ e^- (\gamma)$ final states, track distances from beam axis in DCH planes, and distances between particle impact points at the LKr calorimeter surface were studied. Stability of the results in bins of decay vertex longitudinal coordinate was studied as well. The maximum observed variations of the fit parameters are taken conservatively as the systematic uncertainties.

Background subtraction. For background subtraction in the $\pi^\pm e^+ e^-$ sample the spectra of same lepton sign and $|Q| = 3$ events were used, as described above. This method has a limited statistical precision (with an average of ~ 3 background events in a bin of z). The uncertainties of the measured parameters due to background subtraction were conservatively taken to be equal to the corrections themselves.

Trigger efficiency. As discussed earlier, the corrections for trigger inefficiencies were evaluated by simulations. In particular, L1 and L2 corrections for the measured BR have similar magnitudes of a few 10^{-3}. No uncertainty was assigned to the L1 correction, due to relative simplicity of the trigger condition, and the consequent robustness of the simulation. On the other hand, the uncertainty of the L2 efficiency correction was conservatively taken to be equal to the correction itself.

Radiative corrections. Uncertainties due to the radiative corrections were evaluated by variation of the lower $\pi^\pm e^+ e^-$ invariant mass cut. The results show reasonable stability with respect to the variation, as can be expected given a good MC description of the

Table 1: Corrections and systematic uncertainties (excluding external sources).

Parameter	Particle ID	Beam simulation	Background subtraction	Trigger inefficiency	Radiative corr.	Fitting method
$\lvert f_0\rvert$	0.001	0.006	0.001 ± 0.001	0.002 ± 0.002	0.004	0.003
δ	0.01	0.04	-0.05 ± 0.05	-0.03 ± 0.03	0.04	0.03
a_+	0.001	0.005	-0.001 ± 0.001	-0.002 ± 0.002	0.004	0.004
b_+	0.009	0.015	0.021 ± 0.021	0.015 ± 0.015	0.014	0.010
$\tilde{\mathrm{w}}$	0.001	0.002	-0.002 ± 0.002	-0.001 ± 0.001	0.002	0.001
β	0.06	0.09	-0.09 ± 0.09	-0.06 ± 0.06	0.06	0.04
M_a/GeV	0.004	0.009	0.009 ± 0.009	0.007 ± 0.007	0.009	0.006
M_b/GeV	0.002	0.003	0.004 ± 0.004	0.003 ± 0.003	0.004	0.002
$\mathrm{BR}_{1-4} \times 10^7$	0.02	0.02	-0.02 ± 0.02	-0.01 ± 0.01	0.02	0.02
$\mathrm{BR}_{\mathrm{mi}} \times 10^7$	0.02	0.02	-0.01 ± 0.01	-0.01 ± 0.01	0.02	n/a

$\pi^{\pm}e^+e^-$ radiative mass tail visible in Fig. 2a. Estimation of systematic uncertainties as differences of fit results obtained with radiative corrections calculated using the PHOTOS simulation and the formalism given in [13] leads to similar results as those obtained with the first method.

Fitting method. Uncertainties due to the fitting procedure were evaluated by comparing the fit results obtained with a bin width $\Delta z = 0.01$ with those obtained with the standard bin width of $\Delta z = 0.02$.

External input. Substantial uncertainties arise from the external input, as $\mathrm{BR}(\pi^0_D) = (1.198 \pm 0.032)\%$ is experimentally known with a limited relative precision of 2.7% [14]. The only parameter not affected by this external uncertainty is the slope δ of the linear form factor describing the shape of the spectrum.

The applied corrections and the systematic uncertainties, excluding those from external sources, are summarized in Table 1. Uncertainties due to the external input can be found in Table 2.

3 Results and discussion

The measured value of the model-independent $\mathrm{BR}_{\mathrm{mi}}(z > 0.08)$, as well as the parameters of the considered models and the corresponding BRs in the full z range, with their statistical, systematic, and external uncertainties are presented in Table 2. The 68% confidence level contours for the pairs of parameters corresponding to each model are presented in Fig. 6. The corresponding correlation coefficients between the model parameters are $\rho(|f_0|, \delta) = -0.962$, $\rho(a_+, b_+) = -0.913$, $\rho(\tilde{\mathrm{w}}, \beta) = 0.999$ and $\rho(M_a, M_\rho) = 0.998$.

The measurement of the model-independent $\mathrm{BR}_{\mathrm{mi}}(z > 0.08)$, while not involving extrapolation into the region $z < 0.08$ depending on the form factor parameterization, still relies on the extrapolation into the region of the radiative tail $M_{\pi ee} < 470$ MeV/c^2.

Each of the four considered models provides a reasonable fit to the data (χ^2 of the fits are indicated in Fig. 5a), however the linear form factor model leads to the smallest χ^2. The size of the data sample is insufficient to distinguish between the models.

Earlier measurements of the decay parameters are summarized in Table 3. The present

Table 2: Model-independent $\mathrm{BR}_{\mathrm{mi}}(z > 0.08)$, and fit results for the considered models.

$\mathrm{BR}_{\mathrm{mi}} \times 10^7 =$	2.28	$\pm$	$0.03_{\mathrm{stat.}}$	$\pm$	$0.04_{\mathrm{syst.}}$	$\pm$	$0.06_{\mathrm{ext.}}$	$=$	2.28	$\pm$	0.08
Model (1)											
$\lvert f_0 \rvert =$	0.531	$\pm$	$0.012_{\mathrm{stat.}}$	$\pm$	$0.008_{\mathrm{syst.}}$	$\pm$	$0.007_{\mathrm{ext.}}$	$=$	0.531	$\pm$	0.016
$\delta =$	2.32	$\pm$	$0.15_{\mathrm{stat.}}$	$\pm$	$0.09_{\mathrm{syst.}}$			$=$	2.32	$\pm$	0.18
$\mathrm{BR}_1 \times 10^7 =$	3.05	$\pm$	$0.04_{\mathrm{stat.}}$	$\pm$	$0.05_{\mathrm{syst.}}$	$\pm$	$0.08_{\mathrm{ext.}}$	$=$	3.05	$\pm$	0.10
Model (2)											
$a_+ =$	-0.578	$\pm$	$0.012_{\mathrm{stat.}}$	$\pm$	$0.008_{\mathrm{syst.}}$	$\pm$	$0.007_{\mathrm{ext.}}$	$=$	-0.578	$\pm$	0.016
$b_+ =$	-0.779	$\pm$	$0.053_{\mathrm{stat.}}$	$\pm$	$0.036_{\mathrm{syst.}}$	$\pm$	$0.017_{\mathrm{ext.}}$	$=$	-0.779	$\pm$	0.066
$\mathrm{BR}_2 \times 10^7 =$	3.14	$\pm$	$0.04_{\mathrm{stat.}}$	$\pm$	$0.05_{\mathrm{syst.}}$	$\pm$	$0.08_{\mathrm{ext.}}$	$=$	3.14	$\pm$	0.10
Model (3)											
$\tilde{\mathrm{w}} =$	0.057	$\pm$	$0.005_{\mathrm{stat.}}$	$\pm$	$0.004_{\mathrm{syst.}}$	$\pm$	$0.001_{\mathrm{ext.}}$	$=$	0.057	$\pm$	0.007
$\beta =$	3.45	$\pm$	$0.24_{\mathrm{stat.}}$	$\pm$	$0.17_{\mathrm{syst.}}$	$\pm$	$0.05_{\mathrm{ext.}}$	$=$	3.45	$\pm$	0.30
$\mathrm{BR}_3 \times 10^7 =$	3.13	$\pm$	$0.04_{\mathrm{stat.}}$	$\pm$	$0.05_{\mathrm{syst.}}$	$\pm$	$0.08_{\mathrm{ext.}}$	$=$	3.13	$\pm$	0.10
Model (4)											
$M_a/(\mathrm{GeV}/c^2) =$	0.974	$\pm$	$0.030_{\mathrm{stat.}}$	$\pm$	$0.019_{\mathrm{syst.}}$	$\pm$	$0.002_{\mathrm{ext.}}$	$=$	0.974	$\pm$	0.035
$M_\rho/(\mathrm{GeV}/c^2) =$	0.716	$\pm$	$0.011_{\mathrm{stat.}}$	$\pm$	$0.007_{\mathrm{syst.}}$	$\pm$	$0.002_{\mathrm{ext.}}$	$=$	0.716	$\pm$	0.014
$\mathrm{BR}_4 \times 10^7 =$	3.18	$\pm$	$0.04_{\mathrm{stat.}}$	$\pm$	$0.05_{\mathrm{syst.}}$	$\pm$	$0.08_{\mathrm{ext.}}$	$=$	3.18	$\pm$	0.10

measurement of the linear form factor slope δ is in agreement with the previous ones based on $K^+ \to \pi^+ e^+ e^-$ [7, 8] and $K^+ \to \pi^+ \mu^+ \mu^-$ [15] samples, and further confirms the contradiction of the data to meson dominance models [16] which predict lower values of the slope parameter. The obtained $|f_0|$, a_+ and b_+ are in agreement with the only previous measurement [8]. The obtained values of $\tilde{\mathrm{w}}$ and β are in fair agreement with the fit of the data points [8] performed by the authors of [4] (the value of $M_\rho = 0.77549$ GeV/c^2 [14] is used in our fit; using $M_\rho = 0.7711$ GeV/c^2 as in [4] leads to a central value of $\beta = 3.27$, which improves agreement with [4]). The measured parameter M_a is consistent with the nominal mass of the $a_0(980)$ resonance, while M_ρ is a few % lower than the nominal $\rho(770)$ mass [14].

The branching ratio in the full kinematic range, which is computed as the average

Table 3: Summary of earlier measurements of the form factor parameters and BR with their statistical, systematic, and model-dependence uncertainties. Systematic uncertainties were not evaluated for some measurements; a single statistical uncertainty is presented for these cases.

Decay	$K^+_{\pi ee}$	$K^+_{\pi ee}$	$K^+_{\pi ee}$	$K^+_{\pi\mu\mu}$
Refs.	[6]	[7]	[8, 4]	[15]
δ		$1.31 \pm 0.44 \pm 0.19$	$2.14 \pm 0.13 \pm 0.15$	$2.45^{+1.30}_{-0.95}$
$\lvert f_0 \rvert$			0.533 ± 0.012	
a_+			-0.587 ± 0.010	
b_+			-0.655 ± 0.044	
$\tilde{\mathrm{w}}$			0.045 ± 0.003	
β			2.8 ± 0.1	
$\mathrm{BR} \times 10^7$	2.7 ± 0.5	$2.75 \pm 0.23 \pm 0.13$	$2.94 \pm 0.05 \pm 0.13 \pm 0.05$	

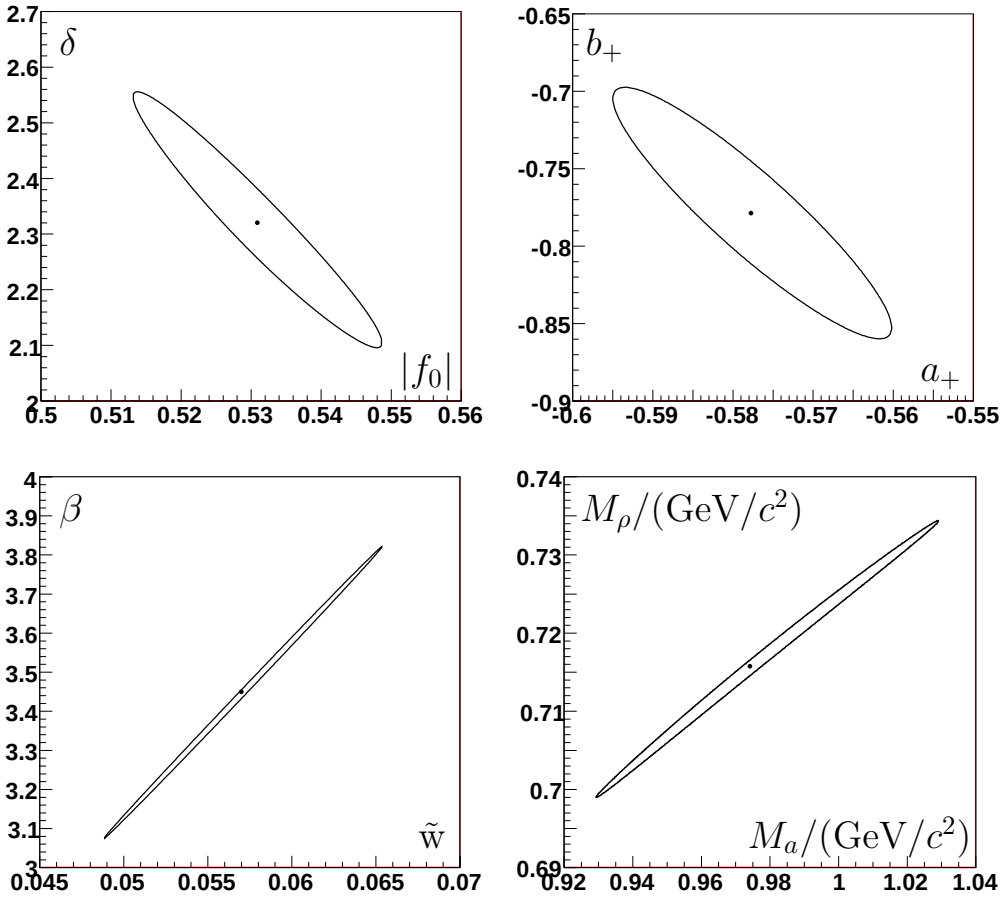

Figure 6: 68% confidence level contours for the parameters of the four models. Only statistical and background subtraction errors are included.

between the two extremes corresponding to the models (1) and (4), and includes an uncertainty due to extrapolation into the inaccessible region $z < 0.08$, is

$$\mathrm{BR} = (3.11 \pm 0.04_{\mathrm{stat.}} \pm 0.05_{\mathrm{syst.}} \pm 0.08_{\mathrm{ext.}} \pm 0.07_{\mathrm{model}}) \times 10^{-7} = (3.11 \pm 0.12) \times 10^{-7}.$$

The uncertainty of the above result is correlated with those of the earlier measurements (those due to external input and model-dependence uncertainties). A comparison to the most precise of these measurements by the BNL E865 collaboration [8] using the same external input, and taking into account correlation of external uncertainties between the two analyses, shows a 1.6σ level of agreement. In conclusion, the obtained BR is in agreement with the previous measurements [6, 7, 8].

Measurements of the decay parameters and BRs were performed separately for K^+ and K^- decays. In particular, the branching fractions in the full kinematic range and their statistical uncertainties were measured to be

$$\mathrm{BR}^+ = (2.99 \pm 0.05_{\mathrm{stat.}}) \times 10^{-7}, \quad \mathrm{BR}^- = (3.13 \pm 0.08_{\mathrm{stat.}}) \times 10^{-7}.$$

This allows making a first measurement of the direct CP violating asymmetry of K^+ and K^- decay rates in the full kinematic range. Considering only the uncorrelated systematic uncertainties (those due to background subtraction) between K^+ and K^- samples,

$$\Delta(K^{\pm}_{\pi ee}) = (\mathrm{BR}^+ - \mathrm{BR}^-)/(\mathrm{BR}^+ + \mathrm{BR}^-) = (-2.2 \pm 1.5_{\mathrm{stat.}} \pm 0.6_{\mathrm{syst.}}) \times 10^{-2}.$$

The other systematic uncertainties are correlated between the K^+ and K^- samples, and thus cancel in $\Delta(K^\pm_{\pi ee})$. A conservative limit for the charge asymmetry of $|\Delta(K^\pm_{\pi ee})| < 2.1 \times 10^{-2}$ at 90% CL can be deduced from the above value. This result is compatible with CP conservation, however the achieved precision is far from the Standard Model expectation $|\Delta(K^\pm_{\pi ee})| \sim 10^{-5}$ [3] and even the SUSY upper limit $|\Delta(K^\pm_{\pi ee})| \sim 10^{-3}$ [17, 18] for the CP violating asymmetry.

Summary

From a sample of 7253 $K^\pm \to \pi^\pm e^+ e^-$ decay candidates with 1.0% background contamination, the branching fraction in the full kinematic range has been measured to be $(3.11 \pm 0.12) \times 10^{-7}$, in agreement and competitive with previous measurements. The shape of the form factor which characterizes the decay has been evaluated in the framework of four models, giving consistent results with previous measurements. The first simultaneous observation of both charge kaon decays into $\pi^\pm e^+ e^-$ allowed to establish an upper limit for the CP violating asymmetry of K^+ and K^- decay rates of 2.1×10^{-2} at 90% CL.

Acknowledgements

We gratefully acknowledge the staff of the CERN SPS accelerator and the beamline for the excellent performance of the beam. We also thank the technical staff of the participating laboratories, universities and affiliated computing centres for their efforts in operation of the experiment and data processing. We are grateful to Samuel Friot, Gino Isidori and Victor Pervushin for valuable discussions.

Appendix

The paper [4] that formulates one of the considered models does not contain the full definition for the form factor $f_V(z)$: the function $\chi(z)$ appearing in the Eq. (3.19) for $f_V(z)$ is defined only below the 2π threshold. The expressions for $\chi(z)$ both below and above the threshold, kindly provided by the authors of Ref. [4], are presented below. Let us define $r = (M_K/m_\pi)^2$. Then for $z < 4/r$ (below the threshold),

$$\chi(z) = \frac{4}{9} - \frac{4}{3zr} + \frac{1}{3}\left(\frac{4}{zr} - 1\right)^{3/2} \arctan\left(\frac{1}{\sqrt{\frac{4}{zr} - 1}}\right),$$

and for $z \geq 4/r$ (above the threshold),

$$\chi(z) = \frac{4}{9} - \frac{4}{3zr} + \frac{1}{6}\left(1 - \frac{4}{zr}\right)^{3/2} \left\{\ln\left(\frac{1 - \sqrt{1 - \frac{4}{zr}}}{1 + \sqrt{1 - \frac{4}{zr}}}\right) - i\pi\right\}.$$

References

[1] S.L. Glashow, J. Iliopoulos and L. Maiani, Phys. Rev. **D2** (1970) 1285.

[2] G. Ecker, A. Pich and E. de Rafael, Nucl. Phys. **B291** (1987) 692.

[3] G. D'Ambrosio *et al.*, JHEP **9808** (1998) 4.

[4] S. Friot, D. Greynat and E. de Rafael, Phys. Lett. **B595** (2004) 301.

[5] A.Z. Dubničková *et al.*, Phys. Part. Nucl. Lett. **5** (2008) 76 [hep-ph/0611175].

[6] P. Bloch *et al.*, Phys. Lett. **B56** (1975) 201.

[7] C. Alliegro *et al.*, Phys. Rev. Lett. **68** (1992) 278.

[8] R. Appel *et al.*, Phys. Rev. Lett. **83** (1999) 4482.

[9] J.R. Batley *et al.*, Eur. Phys. J. **C52** (2007) 875.

[10] V. Fanti *et al.*, Nucl. Inst. Methods **A574** (2007) 433.

[11] GEANT detector description and simulation tool, CERN program library long writeup W5013 (1994).

[12] E. Barberio and Z. Was, Comp. Phys. Comm. **79** (1994) 291.

[13] G. Isidori, Eur. Phys. J. **C53** (2008) 567.

[14] C. Amsler *et al.* (PDG), Phys. Lett. **B667** (2008) 1.

[15] H. Ma *et al.*, Phys. Rev. Lett. **84** (2000) 2580.

[16] P. Lichard, Phys. Rev. **D60** (1999) 053007.

[17] A. Messina, Phys. Lett. **B538** (2002) 130.

[18] G. D'Ambrosio and Dao-Neng Gao, JHEP **0207** (2002) 068.